Proceedings of Meetings on Acoustics

Volume 19, 2013 http://acousticalsociety.org/

ICA 2013 Montreal
Montreal, Canada
2 - 7 June 2013

Musical Acoustics
Session 2aMU: Aeroacoustics of Wind Instruments and Human Voice I

2aMU1. Aeroacoustics of the panpipes

Felipe Meneses, Roman Auvray*, Patricio De la Cuadra, Pierre-Yves Lagrée and Benoit Fabre

***Corresponding author's address: LAM, Institut Jean le Rond d'Alembert, Paris, 75015, Ile de france, France, auvray@lam.jussieu.fr**

The generic term "flute-like instruments" includes a wide variety of instruments whose sound production is ensured by the coupling of an air jet with an acoustic resonator. Within the family, different kinds of resonator may be used with different kind of air supply systems such as the ones found in the recorder or the shakuhachi. It is common to extent the results obtained on one of the member of the family to the whole family. However, when an accurate description of the sound production mechanisms is required, small discrepancies may arise due to the wide variability in the geometries or in the air supply systems. Among other, a closed-end flute may have a different behavior than an open-open flute since the recirculation of air flow within the pipe may alter the hydrodynamics of the jet, and thus the auto-oscillation process. While most of the studies on flute-like instruments have focused on open pipes (organ pipes and recorder), the panpipes (a representative closed-end flute) has only received little attention. We present experimental data, including flow visualization and pressure signal measurement gathered on a closed pipe. Several image processing algorithms to extract informations from the large amount of data are presented.

Published by the Acoustical Society of America through the American Institute of Physics

 [DOI: 10.1121/1.4799950]
Received 22 Jan 2013; published 2 Jun 2013

INTRODUCTION

The acoustic soundscape of pre-hispanic South American cultures is a very rich and unique source of musical information. Different than the Western tradition, the aesthetic guidelines of this music seem largely based on the construction of a collective texture, composed of loud and dissonant sounds of instruments that are pushed to their boundaries [1]. The most prevailing and widespread flute-like instrument in the Andean region is the siku, or zampoña (a name appointed by the Spanish). It consists in several cylindrical closed-end resonators attached together or carved into one solid piece. Its construction is similar to the European panflute, although the siku is used to produce sounds of an extraordinary loud volume. As a result, the air jet is mostly operated on turbulent regime.

The importance of this two characteristics –namely, the closed-end resonator and the turbulent jet– in the sounding mechanisms of this instruments is not clear. On one hand, the speed of the jet is expected to produce turbulences that affect the spread of its shape and the slowing of its central velocity. Thus, the convection velocity of the perturbation along the jet is also affected. Closed-end resonators, on the other hand, produce a well known shift of the impedance maxima, but the fluid dynamical aspects have received little attention. Moreover, there is no evidence of how their joint effect in a real sounding instrument could modify the traditional flute description [2]. For instance, the fluid dynamic balance in stopped pipes might produce an auto-direction effect of the jet towards the labium. It seems that there is no need to aim the jet sharply at the labium to produce a sound, which makes it is easier to play.

Experiments for flow measurement are usually carried out by exciting free, unconfined jets with an external acoustic source [3, 4, 5, 6]. We know this to be a valid approach to study the instabilities of the jet and the evolution of the velocity profile. However, it disregards the jet-labium interaction and the flow balance in the resonator, which is a crucial aspect in stopped pipes. Therefore, it is of interest to bring this matters into a laboratory environment under conditions that are as realistic as possible. The complications of this task are mostly related to the trade off between a neat experimental configuration and a sound production that resembles that of real instruments. This last issue implies several small in-situ modifications that produce images not well suited for analysis. Also, the frequency of oscillation of the jet depends on various geometrical parameters and is very sensitive to the blowing conditions. This means that it cannot be fixed to synchronize the image acquisition rate for a direct representation of the jet oscillations.

In this work we present an experimental procedure for the measurement of some hydrodynamic properties of an air jet in a real instrument configuration. A Schlieren visualization scheme is implemented on a laboratory replica of an Adean siku that is blown with a turbulent jet. An algorithmic routine is developed in order to handle large amounts of data, to semi-automatically transform the raw images into a useful representation of the jet oscillations. Additionally, a technique of aggregation of graphical information is used to lessen the effects of turbulent-related noise, in order to apply algorithms of detection of the jet's centerline with success. As a result, we obtain a time representation of the jet wave.

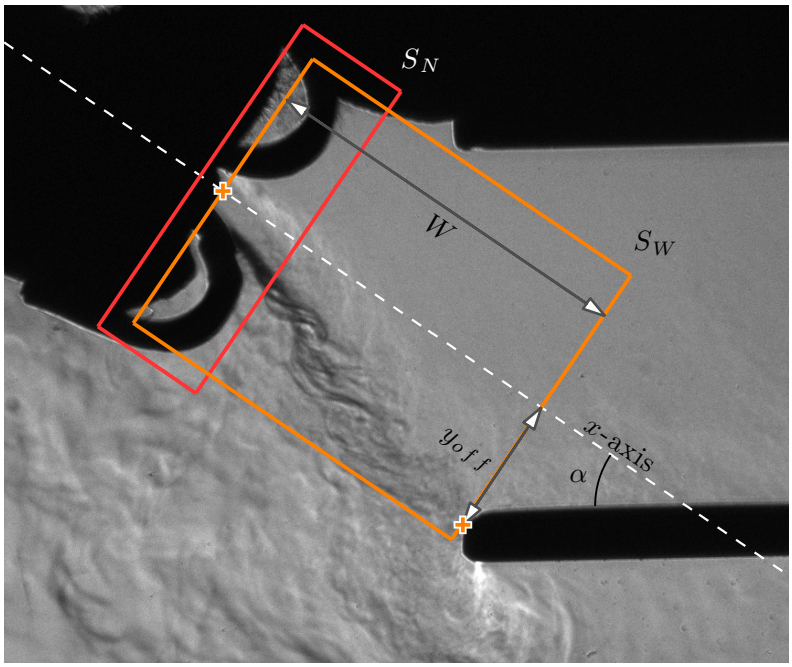

FIGURE 1: Typical image with highlighted attributes of interest.

BASIC FLUTE OPERATION

Sound production in flute-like instruments can be thought of as the coupling between an unstable jet and the resonant modes of a pipe. In resonant operation, the jet, which emerges from the lip of the musician, is surrounded by an acoustic field that perturbs the jet at its flow separation points. Because the jet is basically unstable, a wavy transverse perturbation $\eta(x,t)$ is amplified while convected downstream. At the labium, the jet is split inward and outward. The subsequent out of phase flow injection is usually described as a pressure source – a force driving the air column inside the pipe. The resonator acts as a filter, amplifying the source near its resonant frequencies and creating the acoustic field that closes the feedback loop.

As it is customary in the literature, the x-axis is defined as the initial streamwise direction of the jet. The horizontal projection of the distance from the flue exit –the origin of the oscillations– up to the labium is W, and the orthogonal distance from the labium to the x-axis is the vertical misalignment y_{off}. In this experiments the jet has an inclination α relative to the main axis of the pipe. Figure 1 illustrates this description.

Because the end of the pipe is closed, the inward flow must evacuate through the blowing end. Thus, a static pressure gradient, in addition to the oscillation of the acoustic pressure, is set along the pipe leading to a steady outward flow directed cross-stream to the jet. The jet, while crossing this area, is shifted because of the interaction with the crossflow.

The total displacement of the centerline $\eta(x,t)$ is the sum of the oscillatory $\eta'(x,t)$ and the mean $\langle\eta\rangle(x)$ components. The behavior of the latter will be experimentally investigated. For laminar jets, the perturbation $\eta'(x,t)$ is usually described, in agreement with the linear stability analysis, as a propagative transverse oscillation of the initial perturbation η_0 of the jet centerline [3]:

$$\eta'(x,t) = e^{\alpha_i x}\eta_0(t - x/c_p), \tag{1}$$

where c_p is the phase convection velocity and α_i an amplification parameter.

IMAGE PROCESSING

Experimental setup

A laboratory replica of a siku was built, with the modifications necessary to allow visualization and pressure measurement at the closed-end. A carbon dioxide jet is blown into the pipe to provide mass gradient with the surrounding air, a necessary condition for Schlieren visualization. The experimental arrangement permits to adjust the jet-pipe angle α, the jet-labium misalignment y_{off} and the Reynolds number $Re = u_0 h/\nu$, varied through the jet velocity u_0 – for a slit of heigh h and a fluid of viscosity ν.

The stopped pipe is an aluminum tube of square cross section that provides a fundamental frequency of approximately 690 Hz. In the region near the open end, two opposite walls were cut off and replaced with two larger pieces of transparent glass so as to clear out a visualization area. The round edges of the flue exit attempt to resemble that of a human player. An additional rubber piece is used to seal the gap that is normally filled by the the lower lip of the instrumentalist. The pipe and the nozzle are mounted on a system that allows for the adjustment of the jet-pipe angle α; while the pipe remains fix in a vertical position, the flue exit is allowed to rotate orthogonally to the perimeter of a circle of radius W. This last parameters is adjusted heuristically to produce the adequate sound. A mass flow regulator is used to indirectly control the Reynolds number.

Each experiment consists in the acquisition of N=368 images at a rate of 8 Hz (~ 46 sec) under steady conditions of the control parameters. Turbulent jets on the range $Re \simeq 3000 - 6500$ are investigated, for angles α between 24° and 68°, and for two jet offset configurations y_{off}=0 mm and y_{off}=3 mm. In all cases the instrument is able to produce a defined sound.

Phase detection

The exact sounding frequency f of the pipe is determined by several factors, like the jet velocity u_0 and the flue-labium distance W. The setup arrangement is oriented towards obtaining an optimal sound, which involves several in-situ adjustments; the final value of f cannot be predefined and it varies from one experiment to another. On the other hand, the capture rate of the camera is a fix low rate which makes it impossible to obtain a real-time representation of the phenomenon of interest: the oscillations of the jet. However, since the jet wave is phase-locked to the acoustic oscillations, using the synchronizing signal of the camera make possible to detect the instantaneous acoustic phase ϕ_t at the moment of the capture of each image. As a results, an array of images $I = [I_1, I_2, ..., I_N]$ is linked to a vector of phases $\phi = [\phi_1, \phi_2, ..., \phi_N]$ that are ordered such that $0 \leq \phi_1 \leq \phi_2 \leq ... \leq \phi_N < 2\pi$. In other words, the sequence of images I is a representation of a complete period of oscillation of the jet wave, using images that were captured at different times over a span of ~43 seconds.

Small vortical structures characteristic of turbulence have no relation with the acoustic oscillations; they behave randomly in consecutive images of I. This is seen as noise for the detection of the jet centerline. Aggregating information from phase adjacent images would highlight recurrent structures and would smooth out others. The following procedure combines images in I (pixel-by-pixel) using a Gaussian-weighted average around a phase φ. The results is what we call an aggregated image $\tilde{J}(\varphi)$:

$$\tilde{J}(\varphi) = \frac{\sum_{k=1}^{N} I_k \cdot c_k(\varphi)}{\sum_{k=1}^{N} c_k(\varphi)}, \tag{2}$$

where the coefficients $c_k(\varphi)$ are defined as

$$c_k(\varphi) = e^{-\frac{1}{2}\left(\frac{\phi_k - \varphi}{\zeta}\right)^2}, \tag{3}$$

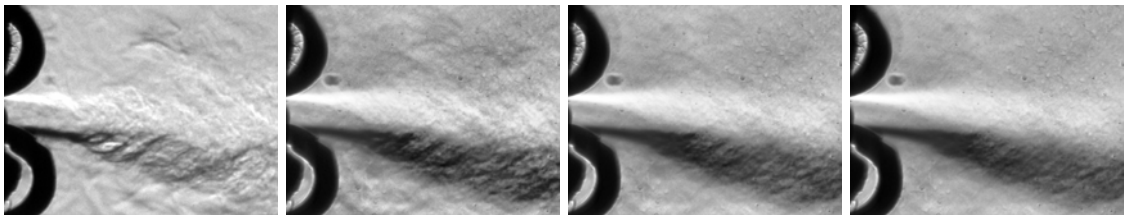

FIGURE 2: Image aggregation process for three different spread parameters ζ and $(Re, \alpha) = (5700, 46°)$.

and the parameter ζ is used to adjust the spread of the curve. Figure 2 shows aggregated images calculated with different parameters ζ. This is an artificial representation where the effects of turbulence are milder, thus favoring the analysis of the centerline.

A reconstruction in time of a period of oscillation of the jet wave is made in T uniform frames $0, \frac{1}{T}2\pi, ..., \frac{T-1}{T}2\pi$. Aggregated images $\tilde{J}(\varphi)$ are computed by forcing φ to match those intervals, and single-shot images J are picked as uniformly as possible from ϕ (with the restriction of the collected data of each experiment). For the following analysis we set $\zeta = 8.4°$ and $T = 32$.

Analysis window

A window of analysis S_W has to be selected, that is invariant between experiments and matches the axes definition of the model (see figure 1). This requires to define an x-axis and a representative point of the origin of the jet. The former cannot be easily deduced from the images: the structure of the nozzle is irregular and the jet contains information of the oscillations and the mean deflection. The total average of the array $\tilde{J}$ of aggregated images is calculated, which is expected to provide a better idea of the initial orientation of the jet. Thereafter, a straight line is manually adjusted to fit the direction of the first stages of the average jet, and the origin is placed at a point where the structure of the nozzle seems to end. This last definition is based solely on graphic considerations and may not coincide with the actual origin of the oscillations. Finally, a representative point at the edge of the labium is manually selected.

The definition of S_W has to bee consistent for different geometrical configurations. The structure of the nozzle is an invariant marker and thus can be used link the window S_W across experiments. An image registration algorithm [8] aligns the nozzle of two images. One is set as a reference, and the other is rotated and translated exhaustively in order to find an optimal pair of windows S_N that maximize the mutual information. Therefore, the window S_W is carefully defined for only one experiment, and the result is extrapolated to the rest by means of the alignment algorithm.

Centerline detection

De la Cuadra[3] proposed an algorithm for measuring the vertical displacement of a jet in an open-end pipe, based on the cross correlation between analog gray profiles of images at consecutive time frames. The method is based on the computation of the crosscorrelation between a reference image at the time frame t_{ref} and the others. Consequently, the estimated displacements are relative to the reference. A brief summary of the algorithm is given below.

The cross correlation of a vertical gray profile $l(y,x,t)$ at a distance x from the flue and for the frame t

$$X(y,x,t) = \int_{-\infty}^{\infty} l(y-\tilde{y},x,t_{ref})l(\tilde{y},x,t)d\tilde{y} \tag{4}$$

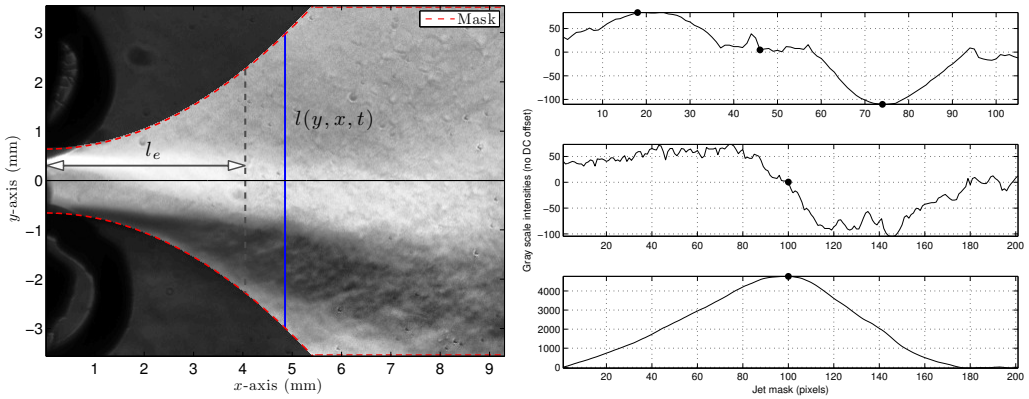

FIGURE 3: Left: Analysis window S_W with quadratic mask used for the centerline detection. Right: Laminar (up) and turbulent (center) gray profiles and integral of a turbulent gray profile (down) used for detection of the centerline.

will have a maximum for a shift $\tilde{y}$ that makes both profiles match best. The relative displacement $\tilde{\eta}(x,t)$ is supposed to be well described by the shift of the maximum from the center of the vector. The resolution is increased using parbolic interpolation of the three highest values.

This operation is repeated for the $T = 32$ time frames and over the entire window $x = 0...W$. The result is stored as a matrix of relative displacements:

$$\tilde{\eta}(x,t) = \begin{pmatrix} 0 & 0 & \dots & 0 \\ \tilde{\eta}_{1,2} & \tilde{\eta}_{2,2} & \dots & \tilde{\eta}_{W,2} \\ \vdots & \vdots & \ddots & \vdots \\ \tilde{\eta}_{1,T} & \tilde{\eta}_{2,T} & \dots & \tilde{\eta}_{W,T} \end{pmatrix}. \tag{5}$$

The first row is filled with zeros to represent the unknown jet position in the reference image.

A typical window of analysis is shown in figure 3 (left). The amplitude of the oscillations and the width of the jet are both larger as the distance x increases. In order to improve resolution of detection, a quadratic mask (red dotted line in figure 3 (left)) is used to select proportionally shorter gray profiles near the flue.

In open pipes, because the mean deflection of the centerline $\langle\eta\rangle$ coincides with the x-axis, the reference displacement is corrected by forcing the mean value of the columns of $\tilde{\eta}(x,t)$ to zero. In closed-end pipes, the position of the jet in the reference image must be obtained separately and then subtracted from $\tilde{\eta}(x,t)$ because $\langle\eta\rangle$ varies with x.

The morphology of the jet in aggregated images is characterized by two velocity profiles (close to a top-hat profile at the exit of the nozzle and Bickley profile far from it). First, the shear layers are two distinguishable boundaries of the jet, and after a distance of development l_e, this boundaries collapse in the centerline. Two algorithms based on the analysis of vertical gray profiles run in the regions $x = [0, l_e]$ and $x = [l_e, W]$, respectively (l_e is selected heuristically). In the first region, $l(y,x,t)$ looks like the upper graph in figure 3 (right). Maximum and minimum points are good indicators of the boundaries of the jet, and the centerline is assumed to lie in the center of both. A gray profile in the second region looks like the center graph in figure 3 (right). Visualization is now characterized by noise, which suggests that a larger scale approach is necessary, such as the area below the curve. This operation acts as a low pass filter, reducing the effects of noise. The integral of the gray profile, starting from the first intensity value, is shown in the lower graph of figure 3 (right). The maximum of this curve marks the centerline.

An exponential fit to the combined results yields the absolute displacement of the reference image $\eta(x,1)$. Finally, the rows of matrix $\tilde{\eta}(x,t)$ have to be corrected by the operation:

$$\eta(x,t) = \eta(x,1) - \tilde{\eta}(x,t), \quad t = 2..T. \tag{6}$$

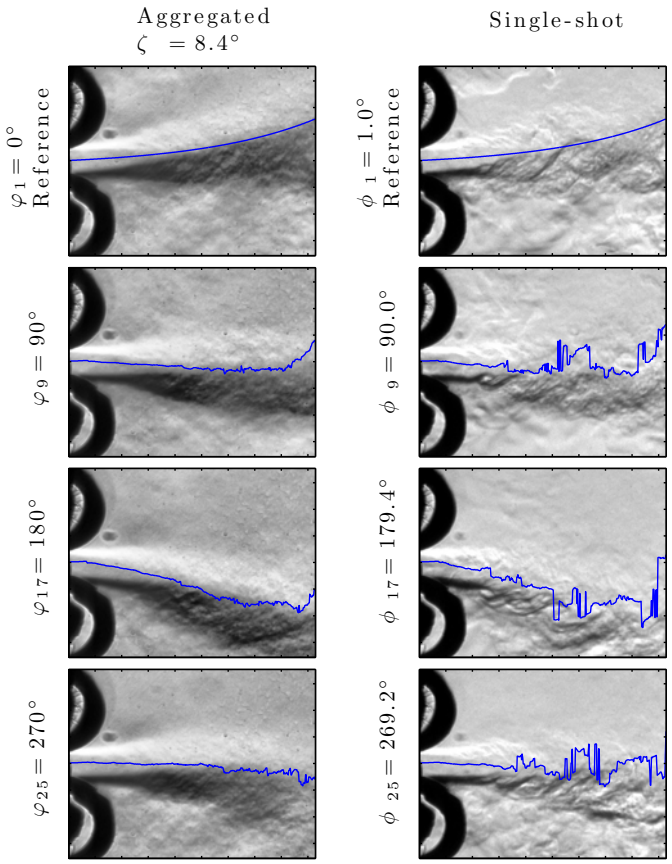

FIGURE 4: Detection of the centerline $\eta(x,t)$ in single-shot and aggregated images for frames $t = [1,9,17,25]$ and $(Re,\alpha) = (5700,46°)$.

The detection of the centerline is illustrated in figure 4.

RESULTS

The static and oscillatory components of the columns of $\eta(x,t)$ represent the mean jet deflection $\langle\eta\rangle$ and the jet wave $\eta'(x,t)$, respectively. If the detection was carried out with success, the columns of $\eta'(x,t)$ are expected to describe a sinusoid, as shown in figure 5 (left). That is the case for aggregated images and also for the laminar section of the jet in single-shot images. For the latter, the effects of turbulence in the shape of small vortical structures make the detection impossible beyond the laminar region, because there is no correlation in this structures between successive frames of J. Therefore, a deviation from a sinusoidal behavior is regarded as a sign of turbulence; the figure of choice is the mean squared error (MSE) between the normalized columns of $\eta'(x,t)$ and their fitted sinusoid. As shown in the lower graph in figure 5 (right), the MSE is low in a segment where the jet is laminar. Near the flue the oscillations are starting to arise and the behavior is irregular, and around 2-3 mm the MSE grows rapidly again. This last change correspond to the transition to turbulence l_t.

Harmonic analysis of $\eta'(x,t)$ is performed in order to obtain the amplitude $|\eta|$ and phase $\angle\eta$ of the jet wave. The spatial growth factor can be obtained by fitting the function $\eta_0 e^{\alpha_i}$ (see Eq. 1) to the amplitude data. In this first approximation, results of are found to be in the expected range of $h\alpha_i \simeq 3$ with no change of behavior in the turbulent transition. The phase $\angle\eta$ is related to the acoustic velocity by [4] $c_p = \omega(d_x \angle\eta)^{-1}$. As shown in teh center graph in figure 5 (right), data is

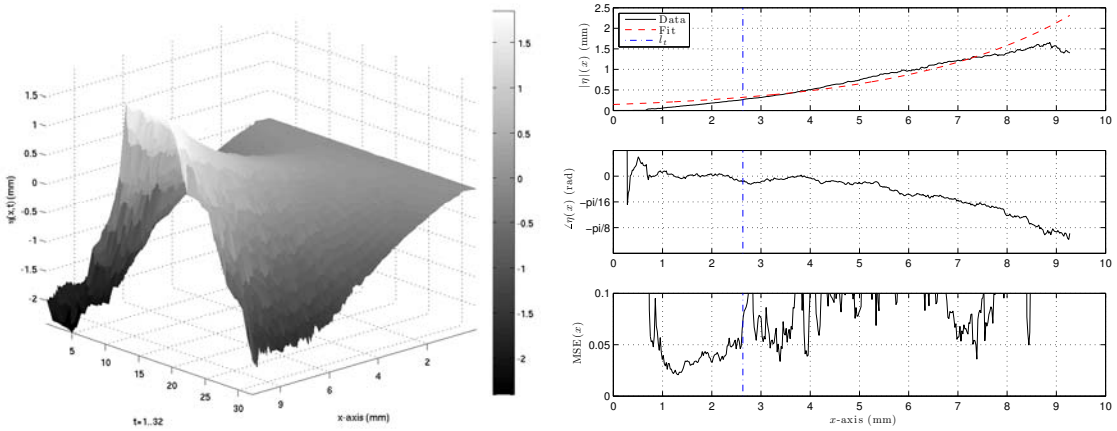

FIGURE 5: Left: three dimensional representation of the jet transverse oscillations $\eta(x,t)$ versus 32 frames and the distance from the nozzle x for $(Re,\alpha) = (5700, 46°)$. As the color bar indicates, the mean value of the oscillations is different than y=0. Right: amplitude, phase and MSE of the oscillations for the blowing condition: (Re,α)=(5700, 46°). The vertical line is the estimation of the transition to turbulence l_t.

irregular in the laminar region and there is a change in the slope of $\angle\eta$ that coincides with l_t.

Since there is no available model for $\langle\eta\rangle$, this experiment serves as a first observation of the overall phenomena. Results shows a tendency of the deflection in the downwards y direction. For $y_{off} \simeq 0$ this tendency ceases when the small initial misalignment is corrected, around $x \simeq W/2$. Contrarily, when $y_{off} \simeq 3$mm, the shifting trend is maintained throughout the whole window. Is seems that the mechanism is such that the total deflection at the labium is $\langle\eta\rangle(W) \simeq y_{off}$

CONCLUSION

The mathematical complexity of the jet dynamics in flute-like instruments makes experimentation the best available way to generate new results [2]. Jet visualization is a non-invasive method that requires expensive algorithmic development in order to extract information that is hidden within the images. Furthermore, detailed flow measurement in actual instruments has proved to be a difficult problem. A series of geometrical and aerodynamical conditions need to be met in order for the instrument to generate an optimal sound, which often collides with experimental restrictions or with the production of data well suited for further analysis.

This article presents a solution to the jet visualization problem and posterior obtainment of flow measurements, applied to the Andean siku. Experiments are carried out without much alteration of the real sounding conditions of the instrument; the work of extracting the practical data is translated to the image processing algorithms. For various Reynolds numbers and jet-angle α configurations, oscillatory and steady information of the centerline can now be extracted, for both laminar and turbulent regions of the jet. Among other, the measurement in a realistic environment of the growth rate α_i of a transversal perturbation of the jet is now within reach. Furthermore, a rough evaluation of the mean centerline deflection is also available and would enable to confirm or to refute the auto-direction effect suggested by Fletcher [7].

The presented tools open the possibility for further studies on the fluid dynamics of the jet in real instruments. This non-invasive and experimentally flexible approach could be applied to other members of the flute family whose sounding mechanisms are not well understood.

REFERENCES

[1] J. P. de Arce, "Sonido rajado: The sacred sound of chilean pifilca flutes", The Galpin Society Journal **51**, 17–50 (1998).

[2] B. Fabre and A. Hirschberg, "Physical modeling of flue instruments: A review of lumped models", Acust. Acta Acust. **86**, 599–610 (2000).

[3] P. de la Cuadra, C. Vergez and B. Fabre, "Visualization and analysis of jet oscillation under transverse acoustic oscillation", J. Flow Visu. & Image Proc. **14**, 355–374 (2007).

[4] A. W. Nolle, "Sinuous instability of a planar air jet: propagation parameters and acoustic excitation.", J. Acoust. Soc. Amer. **103**, 3690–3705 (1998).

[5] S. Thwaites and N. H. Fletcher, "Wave propagation on turbulent jets", Acustica **45**, 175–179 (1980).

[6] S. Thwaites and N. H. Fletcher, "Wave propagation on turbulent jets: II. Growth", Acustica **51**, 44–49 (1982).

[7] N. H. Fletcher, "Stopped-pipe wind instrument: Acoustics of the panpipes", J. Acoust. Soc. Amer. **117**, 370–374 (2005).

[8] F. Maes, A. Collingnon, D. Vandermeulen, G. Marchal and P. Suetens, "Multimodality image registration by maximization of mutual information", Medical Imaging, IEEE Transactions on **16**, 187–198 (1997).